Spin Dynamics of the Pico Satellite Solar Cell Testbed Spacecraft

Siegfried W. Janson
The Aerospace Corporation
Mail Stop M2/241, P.O. Box 92957, Los Angeles, CA 90009-2957; 310.336.7420
Siegfried.w.janson@aero.org

David A. Hinkley
The Aerospace Corporation
Mail Stop M2/241, P.O. Box 92957, Los Angeles, CA 90009-2957; 310.336.5211
David.a.hinkley@aero.org

ABSTRACT

The low Earth orbit (LEO) Pico Satellite Solar Cell Testbed spacecraft (PSSCT; also known as the PSSC Testbed) was ejected from the Space Shuttle Endeavour at 12:34 PM, PST, on November 29, 2008. The LEO PSSCT is a 6.5-kg mass, 5" x 5" x 10", fairly rigid, box-shaped nanosatellite designed to provide space flight data on radiation degradation of multi-junction solar cells. The LEO PSSCT was ejected from the shuttle with the long axis (Z axis) perpendicular to the instantaneous sun-spacecraft line. It has an internal momentum wheel that was spun up before ejection, thus determining the angular momentum vector in inertial space. After ejection, the momentum wheel took 5 minutes to slow down, thus imparting a 507 degree/second rotation rate for the spacecraft body about the Z axis. MEMS rate gyros from Analog Devices were used to monitor the rotation rates about the X, Y, and Z axes, with Earth and sun sensors providing additional information for on-orbit spin rate calibration. The Z axis has the minimum moment-of-inertia, so we expected the spacecraft to transfer energy from the Z axis to the X and Y axes over the course of several months. We obtained over three months of on-orbit spin rate data.

1.0 INTRODUCTION

Explorer-1, launched on January 31, 1958, was the first spacecraft put into orbit by the United States. It had a long pen-shaped body (see Fig. 1) and was injected into orbit with an initial spin of about 11 revolutions per second about the axis of symmetry.[1] Due to the spacecraft geometry and mass distribution, the ratio of maximum to minimum moments of inertia was 75 to 1. The spacecraft was initially spun about the axis of symmetry (minimum moment of inertia), but within one 90-minute orbit, the spacecraft was nutating with a half-angle of about 60°. Spacecraft rotation about different axes was determined by monitoring received radio signal strengths on the ground. The flexible wire antennas converted some rotational energy into heat, and enabled transfer of rotational energy from the minor to the major axes. Since total angular momentum must be conserved in the absence of external torques, the spacecraft began rotating at a slower rate about the minor and major axes. Continued energy dissipation will result in a "flat spin" where the spacecraft rotates primarily about the major axis. The first publication on the tendency of free rotating rigid objects to rotate about the axis of maximum moment of inertia appeared in 1958.[2]

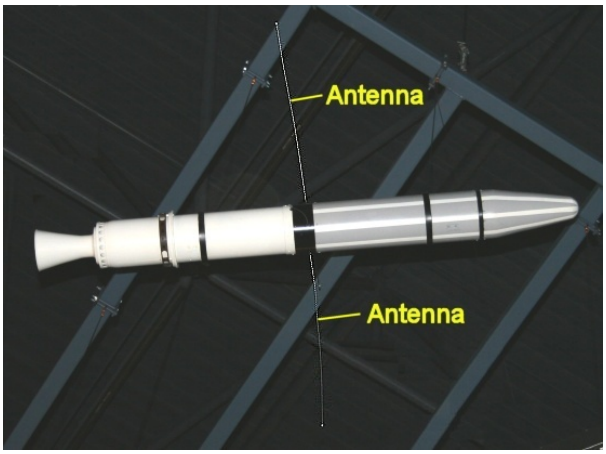

Figure 1. Photograph of Explorer-1 mockup.

The wire antennas were replaced by more rigid antennas on Explorer-III. This spacecraft was launched on March 26, 1958, and it took about a week to go from

an initial 10^o nutation half-angle to 60^o.[1] The growth rate of nutation angle was therefore significantly reduced by eliminating major flexible structures. Now, a little more than 50 years later, we have repeated this experiment using 21st century MEMS rate gyros and miniature attitude sensors on a 6.5-kg mass nanosatellite initially spinning about the "wrong" (minimum moment of inertia) axis. We steadily measured and stored the rotation rates about three orthogonal axes, once every 64 seconds, over a three-month time span. We also occasionally measured rotation rates for 10 minutes with a sample period of 0.193 seconds to eliminate any aliasing. Using these data, the transfer of rotational energy from the minor to major axes, and the loss of overall rotational kinetic energy due to eddy current dissipation within the Earth's magnetic field, were determined.

2.0 THE PSSCT MISSION

The PSSCT mission is designed to monitor accelerated radiation degradation of triple-junction solar cells in a high radiation environment such as geotransfer orbit (GTO). Small satellites provide a rapid turn-around platform, or responsive space flight capability, to flight test new solar cells before they are used on major spacecraft. PSSCT is a nanosatellite because it needs a thick wall all around the electronics as a radiation shield.

A GTO version of PSSCT would sequentially point solar arrays towards the sun while measuring the current-voltage (I/V) characteristic of each array. Total accumulated radiation dose would also be monitored over several energy ranges to track radiation-induced degradation in power output. Solar cells with different formulations could populate different sides of the same PSSCT and directly compete against each other in the same combined effects environment.

To minimize overall mission risk, we added a low Earth orbit (LEO) flight to test on-orbit the key systems, subsystems, and components such as the I/V curve measuring system, the sun sensors, Earth sensors, rotation rate sensors, and magnetic torque coils in a low-radiation environment. There were no radiation sensors on the LEO flight and instead VGA cameras took their place. The satellite had no closed loop attitude control so it was spun-up about its long axis so that each array would face the sun. This serendipitously provided the data for this paper.

The DoD Space Test Program secured a ride on STS-126, and the LEO version of PSSCT was ejected from the Space Shuttle Endeavour at 12:34 PM, PST, on November 29, 2008. Figure 2 shows a photograph of the LEO PSSCT and the Space Shuttle Picosatellite Launcher (SSPL) 5510. This launcher, designed by The Aerospace Corporation and manufactured by Oceaneering Space Systems in Houston, Texas, is a small satellite ejector designed for 5" x 5" x 10" payloads with a mass up to 7 kg. A spring inside the launcher provides a 1 to 2 m/s ejection speed. The SSPL 5510 was first used on STS-116 to eject the RAFT1 and MARScom satellites built by the U.S. Naval Academy and is scheduled for additional use on STS-127.

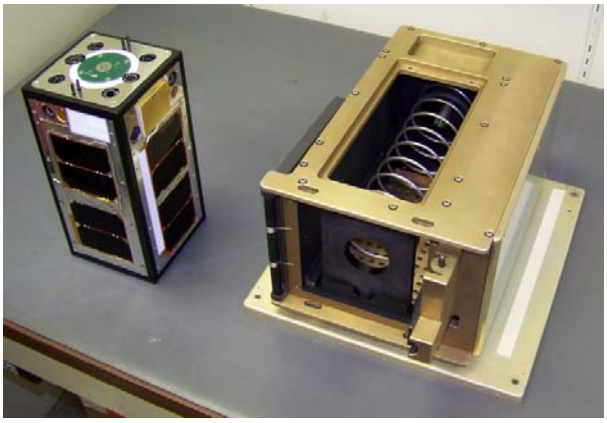

Figure 2. The LEO PSSCT (left) and its launch tube (right).

Figure 3 shows a photograph of the launch tube within the Shuttle bay, and Figure 4 is a photograph of the satellite shortly after ejection. Initial orbital parameters for the LEO PSSCT are 51.6^o inclination and 345-km altitude. Estimated orbital lifetime is about one year.

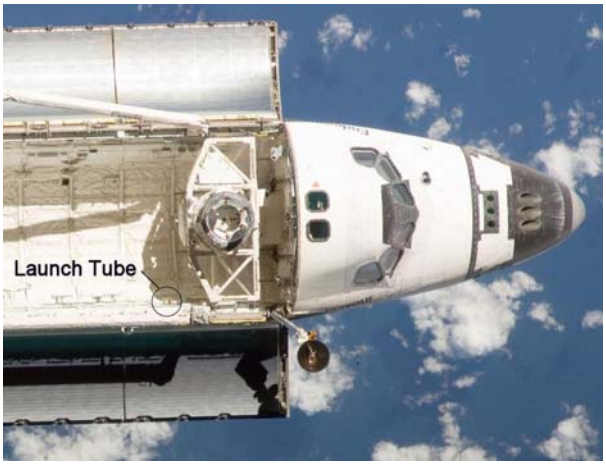

Figure 3. Photograph of our launch tube in the Endeavour payload bay. Photo courtesy of NASA.

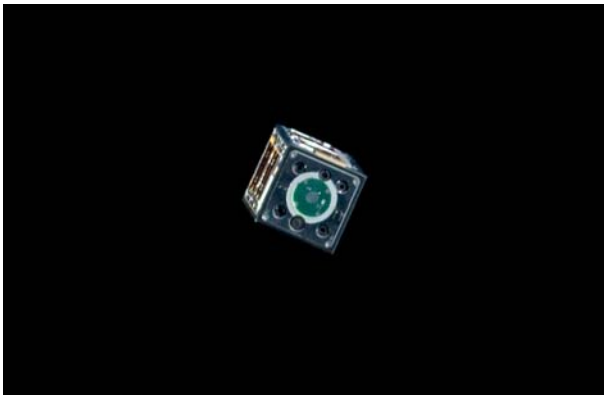

Figure 4. Photograph of the LEO PSSCT after ejection from the shuttle Endeavour. Photo courtesy of NASA.

3.0 PSSCT DESIGN

Figures 2 and 4 show photographs of the satellite while Fig. 5 shows a schematic drawing with reference directions and relevant external components noted. Each 5" x 10" side has a 4-cell solar array and an attitude sensor composed of a two-axis sun sensor and a single pixel infrared Earth sensor. The sun sensor provides the instantaneous solar inclination angle for the associated solar array. The +Z side contains electrical contacts to spin up a single momentum wheel to 5000 rpm while it is still inside the launch tube, and four plungers (switches) that turn on the satellite once it has left the launch tube. This is the side seen in Fig. 4 as the spacecraft moves away from the shuttle. As the momentum wheel slows down, the spacecraft body begins to rotate about the Z-axis. The Z-axis direction in inertial space was chosen to be perpendicular to the sun-Earth vector and normal to the ecliptic. This allowed the 4 solar arrays to sequentially point towards the sun (at least initially) as the spacecraft rotated.

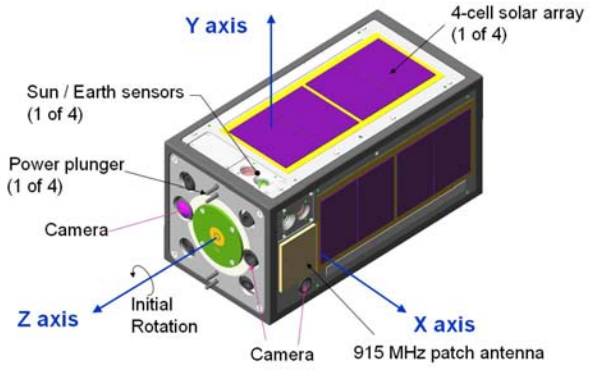

Figure 5. Schematic drawing of the LEO PSSCT.

The LEO PSSCT has a thick aluminum hull to provide a fairly rigid spacecraft shell and radiation shielding for future high radiation orbits. A wall thickness of 0.30" was used to provide a 10-krad interior total dose over a 300-day mission in a 200-km x 35,786-km x 7° GTO orbit.[3] This thick aluminum hull accounts for 50% of the final 6.35-kg spacecraft mass. In addition, the highly conductive shell, coupled with high geomagnetic fields at low altitudes, provided a strong eddy-current based rotation damping mechanism for this LEO PSSCT flight.

3.1 Inertial Sensors

The primary sensors for spin monitoring are ADIS16255 MEMS rate gyros from Analog Devices. These 11.2-mm square by 6.6-mm thick components have a nominal rate range of +/- 320°/second, a temperature coefficient of only 25 ppm/°C, a sensitivity better than 0.1°/sec, and an angular random walk of 3.6°/hr$^{1/2}$ at 25° C.[4] They provide useful rate data up to +/- 600°/second. These chips also provide an integrated angle output, but this feature was not used on-orbit.

Three rate gyros are mounted in orthogonal directions on and within the electronics stack located in the center of the LEO PSSCT. Figure 6 shows a photograph of the stack and the location of one rate gyro and accelerometer. Figure 7 shows an example of the integrated angle output of a stationary, single rate gyro over a ten minute period in the laboratory with a sampling rate of 10 Hz. For this test, the range was set at +/-80°/second. Note that in this test, the integrated angle output varies by less than 3° over a ten minute period. On-orbit, we used the +/- 320°/second range for the first 74 days of operation, and +/- 80°/second thereafter.

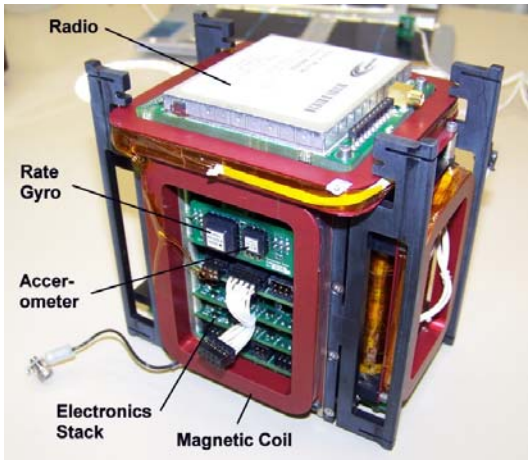

Figure 6. The Electronics Stack.

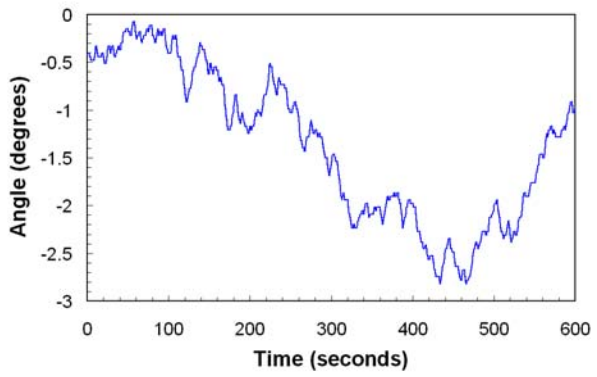

Figure 7. Angle output of a stationary ADIS16255 MEMS rate gyro over 10 Minutes.

The LEO PSSCT also includes three 2-axis Analog Devices ADIS16003 MEMS accelerometers that we use to monitor the proper operation of the rate gyros. These accelerometers have a range of +/- 1.7-g's, a sensitivity of 1.2 milli-g's, and a bias offset of +/- 0.14-milli-g/^{o}C.[5] The accelerometer shown in Fig. 6 is 2.8-cm from the spacecraft axis of symmetry (Z-axis) and can theoretically sense Z-axis rotation rates greater than 0.4^{o}/second at this location. This particular accelerometer provides X-axis accelerations. Another accelerometer, mounted on a circuit board in the main electronics stack, was 2.1-cm from the axis of symmetry, and provides Y-axis accelerations. A third accelerometer, mounted 2.8-cm from the axis of symmetry, provides Z-axis accelerations.

3.2 Attitude Sensors

The LEO PSSCT has three, orthogonal HMC1051ZL single-axis magnetometers from Honeywell. They have a range of +/- 6 gauss with a resolution of 120 μGauss; perfectly useful for determining spacecraft orientation using the Earth's magnetic field in LEO.[6] We discovered during ground testing that the batteries and momentum wheel motors generated significant magnetic disturbances that might prevent the use of magnetic attitude determination. We shielded those components using mu-metal, but the shields still warped the Earth's magnetic field within the spacecraft. (We did not want to add a magnetometer boom because it would reduce the rigidity of the spacecraft.) The magnetic sensors were therefore used only for gross determination of spacecraft orientation.

Our sun sensors each consist of a 200-micron diameter pinhole mounted above a Hamamatsu S7848 two-dimensional position sensitive detector. This design has a +/- 50^{o} angular range in both directions, and an accuracy of +/- 2^{o}.[7] A single sun sensor is mounted on the +X, -X, +Y, and –Y spacecraft sides. More information on their design and operation is provided in reference 7.

Our Earth sensors use a Perkin Elmer TPS333 thermopile as an infrared detector over the 5.5 to 20 micron wavelength range. We experimented with two different configurations. Of the four earth sensors on the spacecraft, one pair uses germanium windows with plastic Fresnel lenses to provide a 30^{o} field of view. They are mounted on the +X and –X faces of the spacecraft. The other pair has a zinc selenide window without focusing to provide a 50^{o} field of view. They are mounted on the +Y and –Y faces.

Inexpensive, low power VGA-resolution image sensors are used to provide pictures of the Earth, and to provide extra attitude information. We use model C328 Comedia camera boards because they have integrated JPEG (Joint Photographic Experts Group) data compression. These 2.0 x 2.8-cm boards have a mass of 10-grams, a maximum power usage of 200-mW, and contain a ¼" 640 x 480 color CMOS imager with a lens. Wide field cameras (123^{o} diagonal) are mounted on the +Z and –X sides, while narrow field (56^{o} diagonal) cameras are mounted on the +Z and +X sides.

3.3 Attitude Actuators

The LEO PSSCT has two identical momentum wheels with spin vectors aligned along the Z axis. The first wheel was spun up to 5,000 RPM while the satellite was in the SSPL 5510 launcher. The spin-up motor was controlled solely by the Shuttle and had no electrical connections to the LEO PSSCT electronics. A second wheel with a maximum spin rate of 6000 RPM, controllable by the LEO PSSCT, was integrated into the spacecraft to provide angular momentum control about the Z-axis once outside the launch tube. Each wheel has a rotational moment of inertia of 2.96 x 10^{-4} kg-m^2 and is driven by a 26-mm diameter brushless DC motor from API Motion. The rotors in these motors have much smaller rotational moments of inertia of 9.4 x 10^{-7} kg-m^2.

Magnetic torque coils were also integrated into the LEO PSSCT to test their attitude control authority. They were only used in open loop control. In the future, they will be integrated into a closed loop attitude control system for the GTO PSSCT. They were not used until February 9, 2009 (mission day 73), when the spin rates of the LEO PSSCT were slow and stable.

3.4 Communications

The LEO PSSCT uses a modified commercial 915-MHz data radio to provide 38.4-kps communications with our 16' diameter ground station antenna in El Segundo, CA. We were able do download over 18 megabytes of data over a three-month period. The spacecraft antenna consists of a single patch antenna designed to provide nearly omnidirectional coverage. This rigid antenna, instead of a deployable flexible antenna, further enhances the structural rigidity of the LEO PSSCT.

4.0 SPIN-UP

Figure 8 shows rate gyro and accelerometer data taken every 0.193 seconds from 10 to 610 seconds after spacecraft activation. The acceleration data are averaged over a one-second interval to reduce the average noise level while the rate gyro data are unprocessed. The spacecraft started with a Z-axis rotation rate of 0°/second while in the launch tube, and reached a rate of 507°/second 295 seconds later. Note that the rotation rate does not asymptotically approach the maximum rate and instead it abruptly stabilizes at the 507°/second rate. This is due to an increase in drag torque in the motor as wheel rotation rate approaches zero. Identical abrupt transition behavior is seen in the rotation-induced radial accelerations measured by the X and Y accelerometers also shown in Figure 8. The difference in final acceleration level between these two acceleration sensors is due to their different distances from the axis of symmetry (0.75 vs. 1.1-cm) and their different bias offsets.

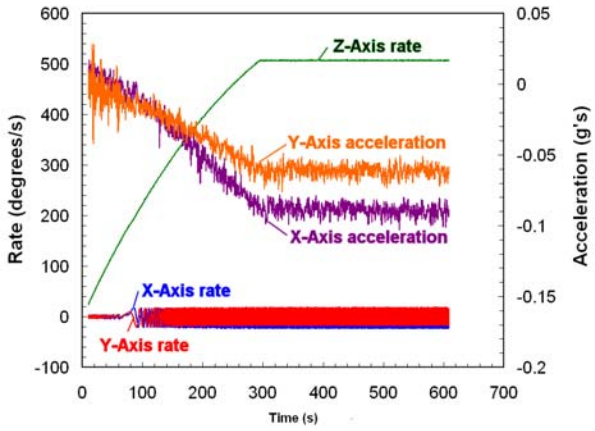

Figure 8. Angular rates and accelerations measured during the "spin-up" phase.

Another interesting feature of the spin up is a sudden increase in spacecraft wobble one minute after ejection. Figure 9 shows the X, Y, and Z rotation rates during the first two minutes after ejection, with X and Y rotation rates changing from about 4°/second to 17°/second near t = 75 seconds. This was probably caused by the physical shift of a component such as the electronics stack, a wiring harness, etc., as the body spun up and internal radial accelerations increased. The axial spin rate was about 180°/second at this point.

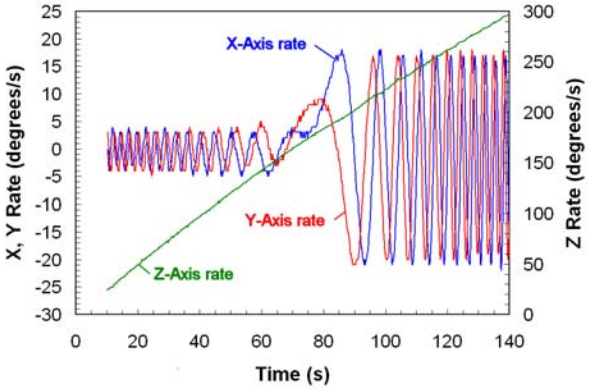

Figure 9. Angular rates measured during the first two minutes of the "spin-up" phase.

Preflight, we estimated the LEO PSSCT moments of inertia with a +/- 10% probable error using rough mass distributions of the major spacecraft systems. The symmetry (Z) and transverse (X and Y) axes had values of 1.7 x 10^{-2} kg-m^2, and 5.1 x 10^{-2} kg-m^2, respectively. Just prior to ejection from the space shuttle, power to arm the SSPL 5510 launcher also spun-up the first momentum wheel (2.96 x 10^{-4} kg-m^2) inside the LEO PSSCT to a preset speed of 5,000 rpm, thereby storing angular momentum. At ejection time, the power to that wheel was cut and by 295 seconds into the flight it had spun-down completely and the LEO PSSCT body was spinning at 507°/second. Therefore, using this data, the actual LEO PSSCT Z-axis moment of inertia is computed to be 1.75 x 10^{-2} kg-m^2.

After 295 seconds, the Z-axis rate in Fig. 8 is stable. Figure 10 shows the X, Y and Z rotation rates at expanded scale between 350 and 362 seconds. Individual data points are shown. The X and Y axes are sinusoidal with a peak-to-peak amplitude of 38° and a period of 1.10 seconds. The X-axis rates lag behind the Y-axis rates by 90° and the X-axis rate sensor appears to have a -4°/second bias offset. Euler's equations with no external torques provide an explanation for this behavior and the ability to determine the spacecraft transverse moment of inertia and nutation angle.

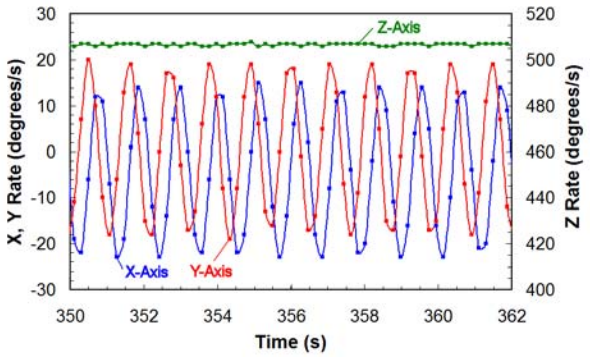

Figure 10. Angular rates and accelerations measured from 350 to 362 seconds.

The basic equations in the principal axis system for a body with $I_{xx} = I_{yy}$ (a reasonable assumption for the box-shaped LEO PSSCT with a square cross-section) with no external torques are:

$$d\omega_x/dt - [(I_{yy} - I_{zz})/I_{xx}]\, \omega_y\, \omega_z = 0 \quad (1)$$

$$d\omega_y/dt - [(I_{zz} - I_{xx})/I_{yy}]\, \omega_z\, \omega_x = 0 \quad (2)$$

$$d\omega_z/dt = 0 \quad (3)$$

The Z-axis rate is constant. Differentiating Eq. 1 with ω_z constant yields:

$$d^2\omega_x/dt^2 - [(I_x - I_z)/I_x]\omega_z \; d\omega_y/dt = 0 \quad (4)$$

Inserting Eq. 2 into Eq. 4 yields:

$$d^2\omega_x/dt^2 + \{[1 - (I_z/I_x)]\, \omega_z\}^2\, \omega_x = 0 \quad (5)$$

Eq. (5) has the solution:

$$\omega_x = A \cos\{[1 - (I_z/I_x)]\, \omega_z\, t\} + B \sin\{[1 - (I_z/I_x)]\, \omega_z\, t\} \quad (6)$$

A similar sequence yields the solution for ω_y:

$$\omega_y = C \cos\{[1 - (I_z/I_x)]\, \omega_z\, t\} + D \sin\{[1 - (I_z/I_x)]\, \omega_z\, t\} \quad (7)$$

Based on the flight data from t = 350 to 362 seconds, A = D = 19.0°/s (0.332 rads/s), B = C = 0, ω_z = 507°/s (8.85 rads/s) and $[1 - (I_z/I_x)]\, \omega_z$ = 328°/s (5.73 rad/s). The last value is the sinusoidal frequency of ω_x. This gives the ratio of the minimum to maximum moments of inertia $I_z/I_x = 0.353$ and $I_x = I_y = 4.96 \times 10^{-2}$ kg-m^2 from spacecraft dynamics.

The total angular momentum L is given by:

$$L^2 = I_x^2\, \omega_x^2 + I_y^2\, \omega_y^2 + I_z^2\, \omega_z^2 . \quad (8)$$

Using Eq. 8 and the data in Fig. 10, we obtain L = 0.156 kg/m^2-s. The nutation angle θ is given by:

$$\cos(\theta) = I_z\omega_z / L \quad (9)$$

which is equal to 6.9° (0.120 radians) over this time span. This is the initial nutation angle after the spacecraft has hit its maximum rotation rate. From now on, the Z-axis rotation rate generally decreases, and the nutation angle generally increases, as rotational energy is transferred from the minimum axis to the maximum axes.

5.0 SPIN-DOWN: FIRST 9 DAYS

Figure 11 shows the Z, X, and Y rotation rates as a function of time for the first 213 hours after ejection from the shuttle. These data were taken using a 64-second sampling period. The Z-axis rate drops from an initial 507°/second to 257°/second after 94.3 hours with an initial Z-axis 1/e decay time of ~140 hours (5.8 days). Over the same period, the X and Y axis rates increase from 19°/second to 107°/second. Note that there are almost 12,000 time samples in Fig. 11, so the oscillatory behavior of the X and Y axes, even though they are significantly undersampled, becomes a solid color. This envelope is used to determine the C and D coefficients in Eqs. 6 and 7 and the nutation angle as a function of time.

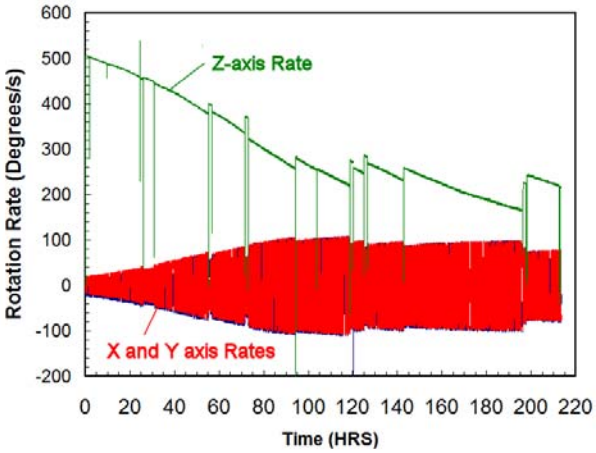

Figure 11. Angular rates measured during the first 213 hours of flight.

The spikes in the Z-axis rates in Fig. 11 occur when we spin-up and down the second Z-axis momentum wheel on the spacecraft. Normally this wheel is powered off, but it can be spun at different rates for variable periods of time in order to stop the satellite body rotation rate and take pictures. We turn it on only when we are over

the El Segundo ground station and only for periods ranging from ten seconds to ten minutes. It can reach 6000 rpm which is fast enough to cause the spacecraft to reverse rotation direction about the Z-axis. The wheel spins-up within 60 seconds but then takes about 3.6 minutes to slow down to a stop which shows up as an almost vertical line in Fig. 11 due to the compressed time scale. Some momentum wheel operations were conducted during sequential ground station passes, resulting in a 1.5 hour separation between some spikes. Most of the time, the Z-axis rate changes after a momentum wheel operation. The X and Y axes rates correspondingly change in the opposite direction with a smaller magnitude. This change in Z-axis rate can be either positive or negative, but the general trend was for positive changes. We are unsure why the change can be positive or negative, but suspect that it may have to do with imperfect Z-axis alignment (it's accurate to +/- 2 degrees) for this momentum wheel.

Figure 12 shows the magnitude of spacecraft body angular momentum L based on the rate data in Fig. 11 and the moments of inertia calculated from the measured on-orbit dynamics. The angular momentum decays smoothly from an initial value of 0.156 kg-m^2/s. The instantaneous angular momentum of the second momentum wheel is not included in this calculation, so wheel operation shows up as a positive or negative spike, depending on polarity of the rotation. Since the angular momentum is decreasing over time, an external torque is acting on the spacecraft. Eddy currents in the conducting spacecraft walls, as they rotated within the Earth's magnetic field, generate this torque (see section 8.0).

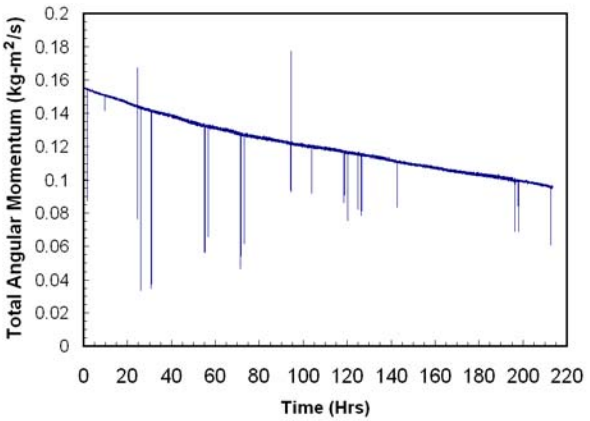

Figure 12. Magnitude of total spacecraft angular momentum during the first 213 hours of flight.

Figure 13 shows the nutation angle for the first 213 hours. It increases from the initial 6.9^o after spacecraft ejection to 60^o at t = 196 hours. This increase is primarily due to energy dissipation within the spacecraft, but external torques could also play a role. Without the intermittent operation of the second momentum wheel, this would have occurred at about t = 120 hours (5 days); a little faster than what was observed in Explorer-III. Unlike the moment of inertia ratio I_{max}/I_{min} of 75 to 1 for Explorer-III, the LEO PSSCT has a much lower ratio of 2.86 to 1. The second momentum wheel was operated multiple times at high speed to reverse Z-axis rotation. These tests are responsible for the nutation angles in excess of 90^o.

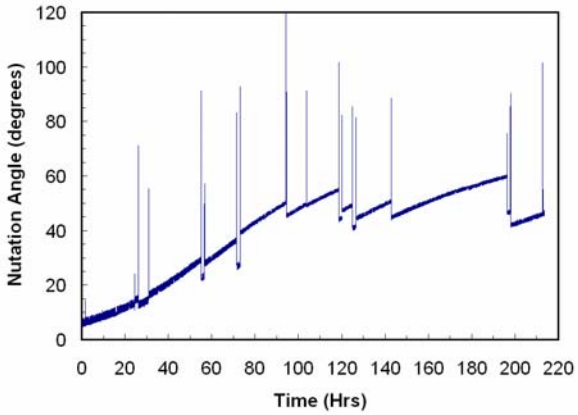

Figure 13. Calculated nutation angle for the first 213 hours of flight.

Figure 14 shows the calculated total rotational energy of the LEO PSSCT for the first 213 hours. Note the decrease in total rotational energy over this same time frame. The initial energy loss rate was 1.3 microwatts and the 1/e decay time for rotational energy loss was ~100 hours (5 days). Spikes due to operation of the second momentum wheel appear, and the rotational energy can shift up or down after wheel operation. Positive spikes occurred when the momentum wheel was spun opposite to the direction of spacecraft rotation while negative spikes are from posigrade rotation. The general trend was increased rotational spacecraft energy after momentum wheel operation. Increases in total rotational energy, coupled with a quasi-stable total angular momentum, would result in decreased nutation angles as shown in Fig. 13.

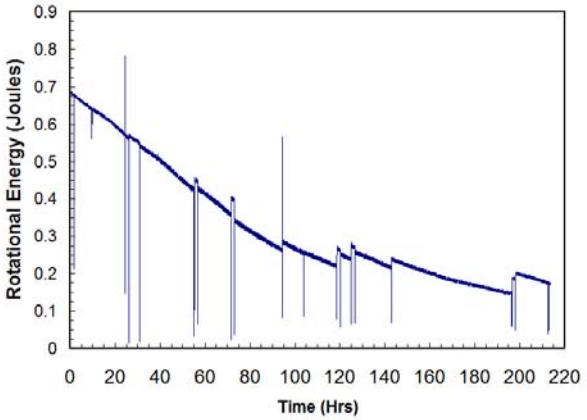

Figure 14. Total rotational spacecraft energy measured during the first 213 hours of flight.

6.0 SPIN-DOWN: THE FIRST 45 DAYS

Figure 15 shows the Z and Y rotation rates over the first 45 days of flight. The Y and X axes were sinusoidal over this time scale, but that structure is not visible at this image scale; there are 60,800 individual time steps shown with occasional data dropouts (also shown). The X-axis envelope is identical to the Y-axis envelope, so it is not plotted. After 25 days of flight, the second momentum wheel was activated less often and fewer discontinuities in the rotation rate data appear. The Z-axis decay rate slows down and the rotation rate at 45 days is 8.2°/second. The Y-axis rates decrease at a much slower pace than the Z-axis. At 45 days, the X and Y axes have peak amplitudes of 20.4° and the LEO PSSCT is primarily in a flat spin.

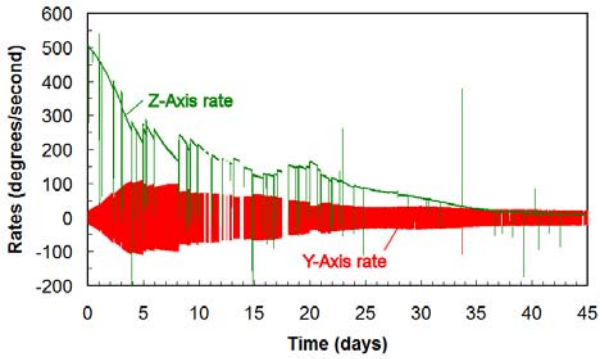

Figure 15. Z-axis and Y-axis rotation rates for the first 45 days of flight .

Figure 16 shows the decay of spacecraft angular momentum over 45 days. The slope of the angular momentum is continuous except for data drop outs and momentum wheel operations. It decays from the initial 0.156 kg-m^2/s value at a slowing rate over time, and has periods of reduced decay between 14 and 18 days, and between 26 and 30 days. Reduced decay rates during these periods are still unexplained.

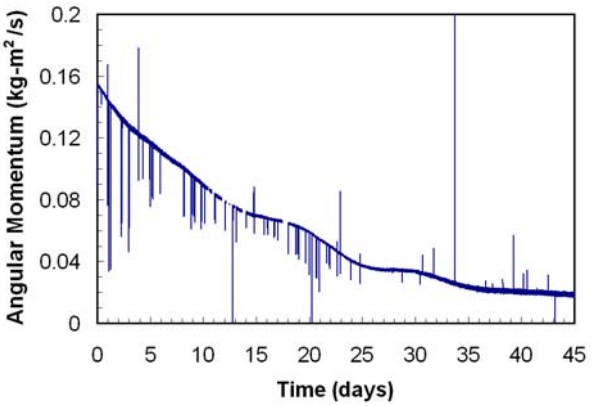

Figure 16. Magnitude of total spacecraft angular momentum during the first 45 days of flight.

Figure 17 shows the calculated nutation angle for the first 45 days. Under ideal conditions, the nutation angle should start at near zero and asymptotically approach 90 degrees. Momentum wheel operation, however, tended to temporarily decrease nutation angles. A significant number of momentum wheel activations between day 9 and day 25 resulted in almost no long term growth in nutation angle. After 25 days with reduced momentum wheel activity, the nutation angle naturally slowly increased to 80°.

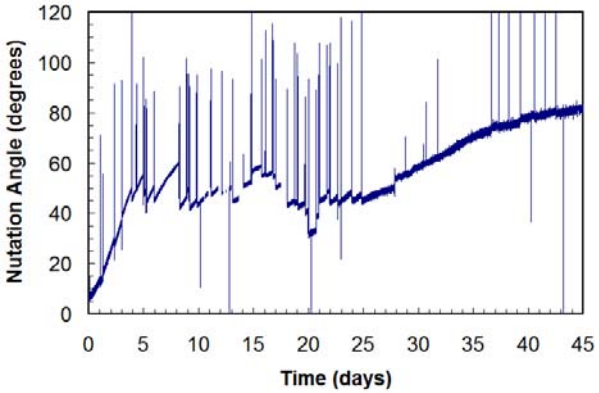

Figure 17. Calculated nutation angle for the first 45 days of flight.

Figure 18 shows the calculated total spacecraft rotational energy for the first 45 days. This was plotted on a logarithmic scale to identify exponential decay rates. An almost linear decline was observed during the first 37 days at a rate of one order of magnitude decrease every 17.2 days. By day 45, the energy loss rate was a mere 2.6 nanowatts.

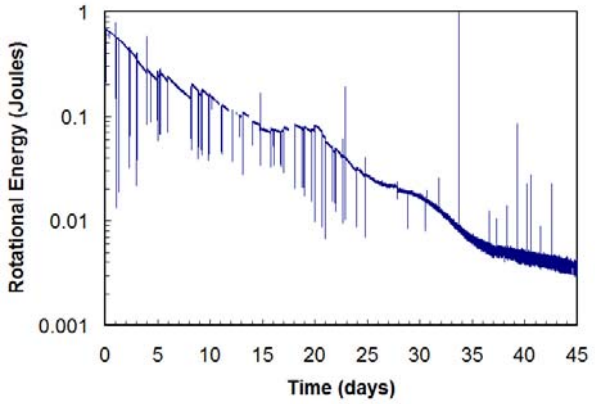

Figure 18. Total rotational spacecraft energy measured during the first 45 days.

7.0 SPIN-DOWN: POST 45 DAYS

The LEO PSSCT provided data for 109 days until March 18, 2009. During the period from 45 to 109 days, the LEO PSSCT was in a flat spin mode and continued to slow down. Figure 19 shows the Z and Y-axis rotation rates from 45 to 90 days while Figure 20 shows the X-axis rate. On day 51, the spacecraft began spinning primarily about the Y-axis for 25 days. Note that we turned on the momentum wheel briefly on day 72 and that reversed the Y-axis rotation rate. X-axis rates generally decreased, with temporary increases after momentum wheel operations. Magnetic torque experiments started on day 73, when rotation rates were low enough to enable real-time torque control. Our spacecraft was now subject to operator-induced changes in spacecraft angular momentum. By day 90, all rotation rates were below 5°/second.

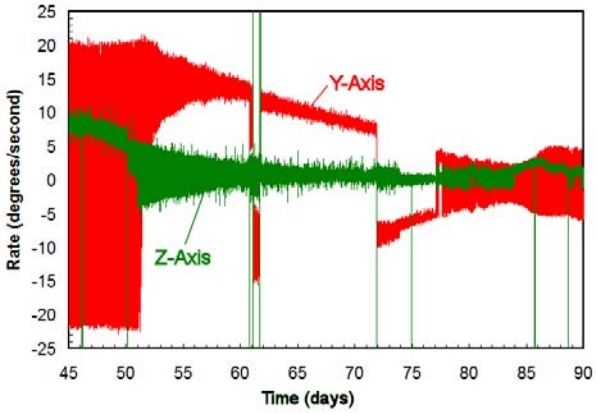

Figure 19. Measured Z and Y-axis rotation rates between 45 and 90 days.

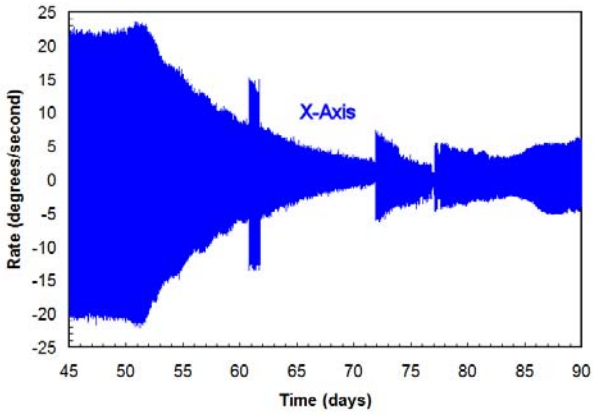

Figure 20. Measured X-axis rotation rates between 45 and 90 days.

8.0 DISCUSSION

Eddy current damping is the logical explanation for the observed rotational energy loss over time. For a flat plate with area A rotating at rate ω within a constant magnetic field B, the maximum electromotive force (EMF) V_{max} occurs around the outer edge with a value:

$$V_{max} = A\,(\partial B/\partial t)_{max} = AB\omega \qquad (10)$$

For a 10" x 5" (25.4 x 12.7-cm) rectangular side of the LEO PSSCT rotating at 507°/second in a 0.3 Gauss magnetic field, V_{max} = 8.6 microvolts. The loop EMF is zero in the center of the plate, so half this value, 4.3 microvolts, is a good estimate of the average loop EMF at $(\partial B/\partial t)_{max}$. Using half of the outer circumference (76.2 / 2 = 38.1-cm) as an average loop length, half the narrow side length (12.7 / 2 = 6.35-cm) as an average loop conductor width, a wall thickness of 0.30" (0.76-cm), and an electrical resistivity of 2.6 microhms-cm for aluminum, we get an estimated loop resistance of 21 microhms. The loop current becomes 120 milliamps and the loop power is 2.6 microwatts at $(\partial B/\partial t)_{max}$. The average EMF is ½ V_{max}, so the average power loss per flat plate is one quarter of the maximum $(\partial B/\partial t)_{max}$ value; 0.65 microwatts. Since individual magnetic field lines go through two plates, the estimated spacecraft eddy current power loss is twice this value, or 1.3 microwatts. This is a crude estimate, based on geometric assumptions made to simplify the calculation that is consistent with the measured initial energy loss rate. Loop EMFs are proportional to ω, so eddy current powers will be proportional to ω^2. After 45 days when the X and Y-axis rotation rates are about 20°/second, the eddy current power loss would be ~2 nanowatts. This is close to the observed value of 2.6 nanowatts.

Therefore, eddy current power losses explain the observed rotational energy decay rates seen in Fig. 18.

The second energy loss mechanism is internal heat generation by flexing structures. The LEO PSSCT is fairly rigid with no flexible external appendages, but inside, the electronics stack is floated for thermal and mechanical shock isolation by thin plastic structures (the blue-gray vertical bars in Fig. 6), and multiple flexible wiring harnesses are used to connect the electronics to sensors and solar cells mounted on the aluminum hull. These can flex and dissipate mechanical energy as heat. By plotting the axial and transverse rotational energies separately in Figure 21, we see that energy transfer from the Z-axis to the transverse axes occurred rapidly during the first 5 days of flight. The maximum rate of transverse energy gain, 0.38 microwatts, occurred between days 2 and 4. Eddy current energy losses were always at least an order of magnitude larger than the energy transfer rate between the Z and transverse axes. Between 9 and 25 days, both the Z and transverse rotational energies declined at similar rates. After 30 days, the transverse energies were greater than the Z-axis energies.

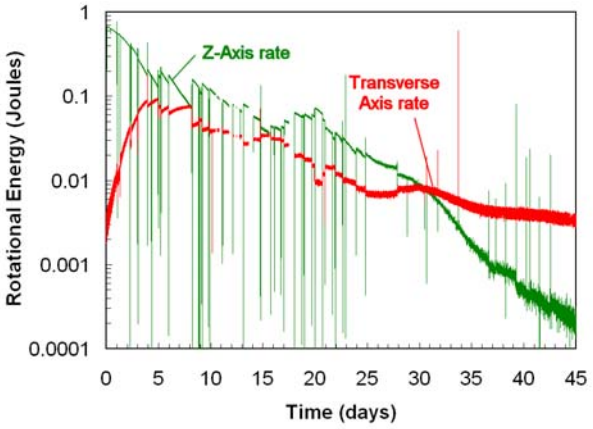

Figure 21. Z-axis and transverse rotational energy as a function of mission time.

A spacecraft with an electrically conducting outer shell will eventually stop rotating due to eddy currents. Spacecraft angular momentum is not conserved, but does the momentum vector remain fixed in direction? We are currently working on determination of the spacecraft angular momentum vector as a function of mission time. The sun sensors provide orientation data as long as the sun passes through their +/- 45° field of view. Unfortunately, we obtained only 7 sets of sun and Earth sensor data over the mission. To augment this data, were are analyzing some of the hundreds of images we obtained from the cameras on board the LEO PSSCT.

We obtained a 72-photo sequence using camera #2 (of four) at 3:48 PM PST on February 10, 2009 (day 74) that illustrates the flat spin. At that time, the X-axis spin rate was sinusoidal with peak-to-peak amplitude of 9.0°/second, the Y axis rate was fairly flat at -7.8°/second, and the Z-axis rate was roughly sinusoidal with a peak-to-peak amplitude of 2.0°/second. Both X and Z axes have a period of 5.0 minutes. Figure 22 shows the recorded angular rate data over a period of 30 minutes. The angular rotation rates were now slow enough to show oscillatory rates using the standard recording rate of one data set every 64 seconds. The spacecraft was in a nutating flat spin about the Y-axis.

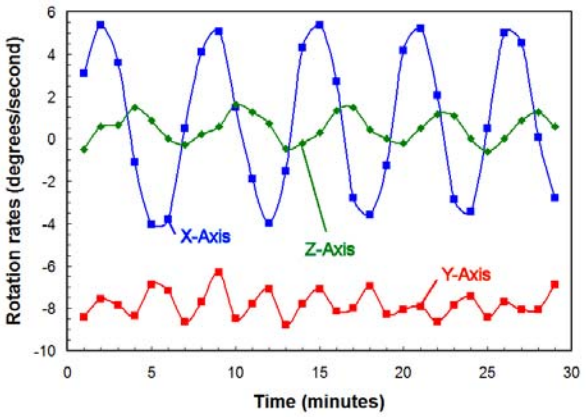

Figure 22. Measured X, Y and Z-axis rotation rates on Feb 10, 2009.

Figure 23 shows the 72 images taken using camera #2. Images are numbered starting with a1 to a9, followed by b1 to b9, etc., and the sequence goes from left to right. The top row is the "a" row and the bottom row is the "h" row. We have no sun or Earth sensors on the +Z or –Z faces, so camera #2 provides sun orientation data. The time between images is a function of image complexity because the camera performs JPEG compression before storing the image, and data storage time is function of data set size. For these images, snapshots are taken approximately every 2-3 seconds. Note that the sun provides a convenient marker in space; the solar disk temporarily overloads individual pixels, resulting in a black output. The centroid of the circular black disk is easily determined on each image.

Figure 23. Image sequence taken on Feb. 10, 2009 at 3:45 PM PST.

Figure 24 shows the location of the sun's centroid on the detector for each image. The first pass (a1 through a6) occurs at an angle, while the third pass (f8 through g3) is almost horizontal.

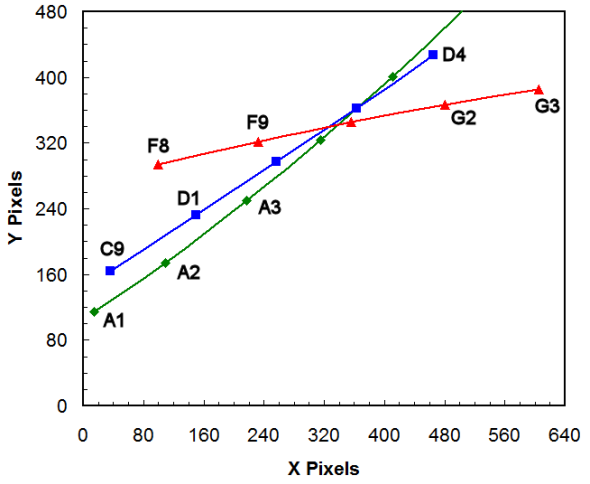

Figure 24. Measured X and Y locations of the sun on the camera image plane.

Figure 24 shows that the spacecraft is rotating about the Y axis (camera #2 was mounted such that it's "X-axis" (640-pixel direction) is along the spacecraft Y-axis). It also shows that by the third pass of the sun (points f8 to g3), the spacecraft Y-axis was almost perpendicular to the Earth-sun line. The spacecraft was still nutating, so the direction of the spacecraft Y-axis was not stationary in inertial space. More analysis is still needed.

9.0 SUMMARY

The LEO PSSCT is solar cell test bed and a precursor to a future GTO PSSCT that will transit the Van Allen radiation belts. The satellite has no active attitude control and was spun up along its minimum moment of inertia axis prior to ejection from the space shuttle in order to stabilize its desired orientation: the long sides of the satellite normal to the Earth-sun line. In addition to performing its solar cell testing mission, the satellite provided valuable spin dynamics information. Its temperature-stabilized MEMS rate gyros measured spin rates to better than 1^o/second and were sampled at 0.016 Hz for the entire mission. It is known that spinning a spacecraft about the axis of minimum moment of inertia eventually results in a transfer of rotational energy from the minimum axis to the maximum axis or axes, but the time constant was unknown for this satellite design. Like Explorer-III, our spacecraft went from a ~6^o nutation angle to ~60^o in about a week. In addition and unexpectedly, the LEO PSSCT also lost momentum rather quickly. The use of a thick aluminum outer shell enhanced eddy-current-induced energy loss rates, applying an external torque. After 77 days on orbit, the LEO PSSCT had gone from a Z-axis rotation rate of 507^o/second to less than 5^o/second on all axes. The eddy current energy loss rates were always an order of magnitude larger than the internal dissipation-induced energy transfer rates from the minimum to maximum axes.

Acknowledgments

We thank The Aerospace Corporation PicoSat team for creating a unique satellite, and particularly Petras Karuza for his assistance in downloading spacecraft flight data and maintaining the flight data records. We also thank The Aerospace Corporation's Independent Research and Development program and its former Corporate Research Initiative in MEMS and Microtechnology for funding research in nano/picosatellites, MEMS for space systems, and parts of The Aerospace Corporation's PicoSat program. We thank SMC/XR for supporting our LEO PSSCT nanosatellite development effort. Finally, we want to thank the Space Test Program, Houston branch and the NASA Payload Safety Review Panel for enabling this flight opportunity for the LEO PSSCT.

References

1. Likins, Peter W., "Effects of Energy Dissipation on the Free Body Motions of Spacecraft," Appendix A, JPL Technical Report No. 32-860, July 1, 1966.

2. Bracewell, R.N., and Garriott, O.K., "Rotation of Artificial Earth Satellites," Nature, 182, pp. 760-762, Sept. 20, 1958.

3. Simburger, E. J., Liu, S., Halpine, J., Hinkley, D., Srour, J.R., Rumsey, D., and Yoo, H., "Pico Satellite Solar Cell Testbed (PSSC Testbed)," 2006 IEEE 4th World Conf. on Photovoltaic Energy Conversion, Vol. 2, pp. 1961-1963, May 2006.

4. Analog Devices, ADIS16250/16255 programmable low power gyroscope data sheet, Analog Devices, Norwood, Massachusetts, URL: http://www.analog.com/static/imported-files/data_sheets/ADIS16250_16255.pdf , 2008.

5. Analog Devices, ADIS16003 Dual-Axis Accelerometer data sheet, Analog Devices, Norwood, Massachusetts, URL: http://www.analog.com/static/imported-files/data_sheets/ADIS16003.pdf , 2007.

6. Honeywell, HMC1051/1052/1053 Magnetic Sensors Datasheet, URL: http://www.ssec.honeywell.com/magnetic/datasheets/HMC105X.pdf , 2006.

7. Siegfried W. Janson, "Micro/Nanotechnology for Picosatellites," paper SSC08-VII-6, Proc. of the 22nd Annual USU Conference on Small satellites (Logan Utah, 2008).